

**Association, Blockage, and Handoffs in IEEE 802.11ad-Based 60-GHz Picocells  
A Closer Look**

Joshi, Kishor Chandra; Hersyandika, Rizqi ; Venkatesha Prasad, R.

**DOI**

[10.1109/JSYST.2019.2937568](https://doi.org/10.1109/JSYST.2019.2937568)

**Publication date**

2020

**Document Version**

Final published version

**Published in**

IEEE Systems Journal

**Citation (APA)**

Joshi, K. C., Hersyandika, R., & Venkatesha Prasad, R. (2020). Association, Blockage, and Handoffs in IEEE 802.11ad-Based 60-GHz Picocells: A Closer Look. *IEEE Systems Journal*, 14(2), 2144-2153. Article 8839948. <https://doi.org/10.1109/JSYST.2019.2937568>

**Important note**

To cite this publication, please use the final published version (if applicable).  
Please check the document version above.

**Copyright**

Other than for strictly personal use, it is not permitted to download, forward or distribute the text or part of it, without the consent of the author(s) and/or copyright holder(s), unless the work is under an open content license such as Creative Commons.

**Takedown policy**

Please contact us and provide details if you believe this document breaches copyrights.  
We will remove access to the work immediately and investigate your claim.

# Association, Blockage, and Handoffs in IEEE 802.11ad-Based 60-GHz Picocells—A Closer Look

Kishor Chandra Joshi , *Member, IEEE*, Rizqi Hersyandika, and R. Venkatesha Prasad , *Senior Member, IEEE*

**Abstract**—The link misalignment and high susceptibility to blockages are the biggest hurdles in realizing 60-GHz-based wireless local area networks (WLANs). However, much of the previous studies investigating 60 GHz alignment and blockage issues do not provide an accurate quantitative evaluation from the perspective of WLANs. In this article, we present an in-depth quantitative evaluation of commodity IEEE 802.11ad devices by forming a 60-GHz WLAN with two docking stations mimicking as access points (APs). Through extensive experiments, we provide important insights about directional coverage pattern of antennas, communication range, and cochannel interference and blockages. We are able to measure the IEEE 802.11ad link alignment and association overheads in absolute time units. With a very high accuracy (96%–97%), our blockage characterization can differentiate between temporary and permanent blockages caused by humans in the indoor environment, which is a key insight. Utilizing our blockage characterization, we also demonstrate intelligent handoff to alternate APs using consumer-grade IEEE 802.11ad devices. Our blockage-induced handoff experiments provide important insights that would be helpful in integrating millimeter wave-based WLANs into future wireless networks.

**Index Terms**—IEEE 802.11ad, 5G, millimeter wave, WiGig.

## I. INTRODUCTION

**D**UE to the availability of a large bandwidth in the millimeter wave (mmWave) frequency band (30 to 300 GHz), it has become a key enabler for providing multi-Gbps wireless access in future 5G-and-beyond networks [1], [2]. In particular, the 60-GHz band has been of special interest for high-speed wireless local area networks (WLANs) [3]. Comparing with the 2.4/5 GHz bands, mmWave propagation is subjected to a very high free-space path loss. For example, path loss at 60 GHz is at least 20 dB more than that at 5 GHz [2]. Directional antennas are used to compensate for the high path loss. Another important propagation characteristic of mmWave signals is the susceptibility to blockage by obstacles, e.g., the human blockage can result in an attenuation up to 20 dB [4].

The existing 60-GHz commercial off-the-shelf (COTS) devices have mainly employed WiGig (IEEE 802.11ad) specifi-

cations [5]. The literature on the experimental evaluations of IEEE 802.11ad based devices is limited and mainly focused on the isolated link characterization measuring throughput, packet structures and received signal strength, attenuation due to obstacles, etc. For example, Zhu *et al.* [6] and Saha *et al.* [7] have used Wilicity's IEEE 802.11ad hardware to investigate the throughput, communication range, blockage-induced attenuation, and beam-steering capabilities in outdoor and indoor environments, respectively. Similarly, Nitsche *et al.* [8] also used Wilicity's IEEE 802.11ad hardware and provides important insights on the imperfections of antenna radiation patterns, interference caused by side lobes, and the dynamics of frame aggregation mechanism. There are very few works [9]–[12] providing important insights on the overheads related to beam-searching, misalignments, and beamwidth adaptations. However, use of customized hardware and software makes it difficult to benchmark the characteristics of commodity IEEE 802.11ad systems. Thus, there is little understanding of how the special characteristics of 60-GHz systems (e.g., directionality, blockage by obstacles, beam alignment) affect the prospect of providing seamless WLAN and cellular communication.

The *major gaps* that exist vis-à-vis the evaluation of commodity IEEE 802.11ad devices are as follows.

- 1) Throughput degradation due to the antenna alignment is investigated but an actual assessment of rebeamforming in absolute time units is missing.
- 2) The spatial reuse capacity of 60-GHz links is highlighted in the literature but the impact of “deafness” arising due to the inability of narrow beam antennas to sense each others' transmissions in IEEE 802.11ad has not received much attention, except in [8].
- 3) Link blockage investigations are limited to the measurement of attenuation in received signal quality, but the link behavior for different types of blockages (i.e., temporary and permanent) and their impact on providing seamless WLAN/cellular experience is not pursued.
- 4) Experimental investigations on the handoff in 60-GHz networks with multiple access points (AP)/base stations (BS) employing COTS IEEE 802.11ad devices has not been attempted so far.

Although the first generation of COTS 60-GHz devices were mainly developed as a replacement of HDMI cables, a wide adoption of 60-GHz technology for WLANs and mobile communications is imminent in the future 5G-and-beyond wireless systems. Therefore, in this article, we evaluate the performance of IEEE 802.11ad devices from a WLANs/picocell

Manuscript received December 3, 2018; revised April 14, 2019; accepted May 23, 2019. Date of publication September 16, 2019; date of current version June 3, 2020. (*Corresponding author: Kishor Chandra Joshi.*)

K. C. Joshi is with the CNRS/CentraleSupélec, University of Paris-Saclay, Saint-Aubin 91190, France, and TU Delft, 2600 GB Delft, The Netherlands (e-mail: k.chandra@tudelft.nl).

R. Hersyandika is with the Spectrum Monitoring Department, MCIT, Jakarta 12550, Indonesia (e-mail: rizqi\_hersyandika@postel.go.id).

R. V. Prasad is with the TU Delft, 2600 GB Delft, The Netherlands (e-mail: r.r.venkateshaprasad@tudelft.nl).

Digital Object Identifier 10.1109/JSYST.2019.2937568

perspective aiming to fill the above listed gaps. We use INTEL's IEEE 802.11ad chipsets instead of the Wilocity chipsets used in [6]–[8]. Our carefully designed experimental scenarios coupled with extensive measurements provide important insights on the misalignment overhead, device discovery/association times, the impact of human blockage, and presence of alternate non-line-of-sight (NLOS) path on the 60-GHz links. We summarize here our main contributions.

- 1) Using extensive measurements, we provide for the first time, an actual estimate of the device association and alignment times in IEEE 802.11ad systems.
- 2) We show that the deafness arising due to the use of directional antennas in 60-GHz communications can heavily deteriorate the link performance.
- 3) We propose a novel human blockage characterization mechanism that differentiates—with a very high accuracy (up to 96%–100%)—the different types of human blockages.
- 4) This is the first article that creates and studies an IEEE 802.11ad-based WLAN system with multiple APs and evaluates the blockage and mobility triggered handoff performance.

The rest of the article is organized as follows. In Section II, we discuss related works. Section III provides the basic characteristics of used COTS devices. We investigate the beam alignment and association overheads in Section IV, which is followed by cochannel interference characterization in Section V. The human blockage characterization, blockage induced handoffs, and mobility induced handoffs are presented in Section VI. Section VIII concludes this article.

## II. RELATED WORKS

Performance evaluation of commercially available IEEE 802.11ad-based systems has received much attention in recent years. Feasibility of 60-GHz outdoor picocells employing Wilocity's 802.11ad chipsets is explored in [6]. Zhu *et al.* show that it is indeed feasible to use 60-GHz band for high data rate communications in outdoor picocells despite the high path loss, susceptibility to blockages by obstacles, and movements induced beam switching resulting in link outages. Investigation on throughput and communication range of 60-GHz radios using Wilocity IEEE 802.11ad chipset is presented in [13] and [7]. It is argued in [13] that relays can significantly improve the performance of IEEE 802.11ad systems.

Ansari *et al.* [14] have measured the bit error rates and throughput performance of various 60-GHz transceivers, which are used for empirical characterization of 60-GHz links. Nitsche *et al.* [8] provide important insights into the frame-level protocol analysis of 60-GHz links using Dell D5000 (which employs Wilocity chips) and WiHD-compatible DVDO Air-3c system as transmitters and Vubiq 60-GHz system receiver to capture the over-the-air transmissions. It is shown that side lobes can result in significant interference up to 5 m distance. It is shown that even a small link misalignment can significantly degrade the throughput neighboring links. Using Dell D5000 docking stations and Dell Latitude E7440 (using Wilocity WiGig chipsets),

Loch *et al.* [15] proposed to use frame aggregation to counter the frame loss due to collisions when multiple 60-GHz links operate simultaneously. In [16], fast beam training and tracking mechanisms are proposed by employing hybrid analog–digital transceivers to simultaneously collect the channel information from multiple directions.

Antenna misalignment and beam searching overheads have extremely adverse effects on the performance of 60-GHz links and can lead to a significant degradation in the link throughput [9]. Simic *et al.* [17] performed measurements in indoor and outdoor environments and argued that misalignment can result in frequent outages. Using customized programmable 60-GHz radio platform called WiMi, Sur *et al.* [10] proposed BeamSpy, an algorithm to predict the quality of alternative beams to reduce beam searching overhead. Zhang *et al.* [11] have proposed LABA: a learning-assisted beam-adaptation mechanism to minimize the beam searching overhead, which is implemented on OpenMili, the next generation of WiMi. Haitham *et al.* [12] have implemented a beam alignment protocol on customized 60-GHz software-defined radio platform that uses sparse-recovery theory to minimize the beam-search space and results in fast beam switching. Haidar and Knightly [18] have proposed MOCA, that invokes beam sounding before each time a packet is transmitted to estimate the link quality of selected beams, to increase the link mobility resiliency. In [22], link blockage evaluation considering mobile and static blockages is presented, however, its impact on handoffs is ignored.

The works listed above have three major limitations: First, most of these papers investigate the performance of 60-GHz systems from the perspective of a single link. On the other hand, we investigate the IEEE 802.11ad systems from a dense WLANs or picocellular system perspective where frequent handoffs can be a major challenge due to the mobility or blockages. Second, previous works on human blockage are merely limited to finding how much signal attenuation is caused by a blocking person. However, we analyze the dynamics of human shadowing in detail, which is highly important in facilitating the handoffs in 60-GHz dense WLANs and picocellular networks. Third, an accurate estimate of alignment time is missing in the literature for the COTS IEEE 802.11ad devices, while we provide accurate estimates of beam alignment and initial user association times for IEEE 802.11ad COTS chipsets.

## III. PRELIMINARY SYSTEM CHARACTERIZATION

We use INTEL WiGig sink chipset W13100 [19] as the AP and a Dell laptop equipped with INTEL tri-band wireless-AC 17265 [20] wireless card as the wireless station (STA). It uses IEEE 802.11ad Control PHY (MCS 0) for control frame transmissions and Single Carrier PHY (MCS 1–12) for the data transmission supporting the data rate in the range of 385–4620 Mb/s. An application programming interface (API) provides the normalized signal quality parameter in the scale of 0 to 10 which indicates the link quality. The lower layer (PHY and MAC) information is not exposed to users, which is the biggest limitation of all commercially available first generation IEEE 802.11ad



Fig. 1. INTEL's WiGig sink chipset W13100.

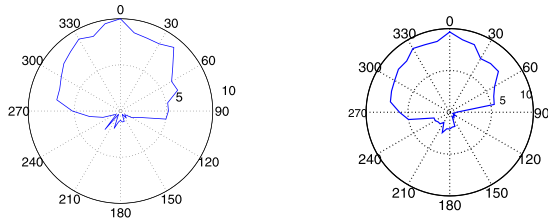


Fig. 2. Directional (azimuth) coverage measurements. (a) Access point's coverage pattern. (b) Laptop's coverage pattern.

chipsets [6]–[8]. In our experiments, we primarily depend on two parameters: 1) normalized signal quality provided by the WiGig API; and 2) throughput measured using the iPerf client [22].

We represent the signal quality parameter with  $q$ , where  $q \in [0, 10]$ . A Dell Latitude-E6430 hosting iPerf server generates the TCP traffic and is connected to the WiGig sink chipset W13100 via Gigabit Ethernet interface. This connection limits the maximum data rate to 1 Gb/s due to the limitation of Gigabit Ethernet port used. Despite the limitations of the experimental setup, we provide powerful insights on the behavior of 60-GHz WLAN/pico cellular network with extensive experiments that are carefully designed to catch the key characteristics of mmWave links in a WLAN scenario.

### A. Directional Coverage Pattern

The first step in characterizing the WiGig chipsets is measuring the coverage patterns of the  $2 \times 8$  antenna array embed in the INTEL's chipsets. Initially, both the AP and STA are positioned 4 m apart in such a way that the antenna array modules face each other ensuring line-of-sight (LOS) connection. To measure the directional coverage in azimuth plane, one device is rotated  $360^\circ$  in a step of  $10^\circ$  while the other is kept fixed and the signal quality " $q$ " is recorded at each  $10^\circ$  steps.

Fig. 2(a) and (b) shows the directional coverage measurements of the AP and the STA, respectively. The results show that antenna arrays of both AP and STA have a nonuniform radiation pattern (antenna gains) in  $360^\circ$  azimuth plane. It is indicated by the high signal quality monitored within  $90$  to  $270^\circ$  angle. This shows the limitations of cost-effective designs used in consumer-grade IEEE 802.11ad chipsets resulting in a skewed coverage in  $360^\circ$  azimuth plane.

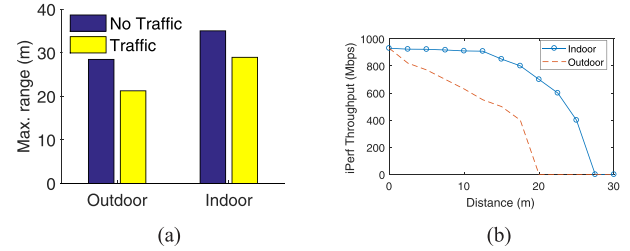


Fig. 3. Maximum communication range and data rates. (a) Communication range. (b) Data rates versus distance in indoors.

### B. Communication Range

To measure the communication range performance (distance) of IEEE 802.11ad AP, we performed experiments in both indoor and outdoor environment. Indoor environment consists of a narrow corridor of width 2 m with hard concrete walls on both the sides, while the outdoor environment consists of an empty park. There were no obstacle between STA and AP. We considered two cases, namely, with the data traffic (using iPerf connection), and without the data traffic (only control traffic related to beaconing, etc., was present). As the distance from AP increases, the signal quality  $q$  received by STA decreases. At a certain distance, STA is disconnected from AP due to the lack of sufficient received signal strength, or data transmission is aborted as the minimum data rate cannot be supported. This distance is referred as the maximum communication range. Fig. 3(a) shows that the maximum range obtained in indoor environment is higher than that in the outdoor environment. Since indoor environment consists of narrow corridor, the reflections through the corridor walls reinforce the LOS component which boosts the communication range. Fig. 3(b) also shows the data rates in indoor (corridor). In each environment, the maximum range is always greater in the absence of data traffic because only the control PHY (MCS0) is used in this case. On the other hand, when data traffic is present, higher MCSs are used that requires greater received signal levels to maintain the connectivity.

## IV. ASSOCIATION AND BEAM ALIGNMENT OVERHEADS

### A. Association

Initially, when the STA is not yet connected to the AP, the measured signal quality  $q$  is zero. After the STA receives the first beacon, the association process begins. We measured the time difference between the first registered signal value and the final stable signal value, which is defined as association time.

An example of signal quality  $q$  during the association process is depicted in Fig. 4(a). In Table I, we show the association time for different distances—1, 4, and 10 m. The measurement results show that the average association time is around 240 ms. Twenty repetitions were performed for each AP-STA distance value. The average association time for all the three distances is almost equal which is logical because IEEE 802.11ad uses two-stage fixed beamwidth searching mechanism.

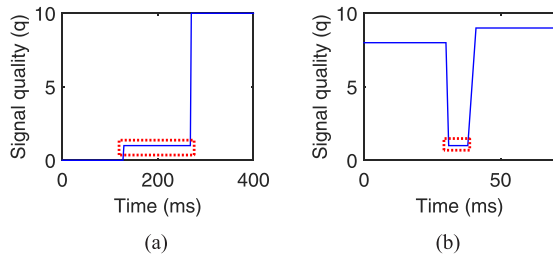


Fig. 4. Snapshot of signal quality variation during association and beam realignment. (a) Association time. (b) Beam realignment.

TABLE I  
IEEE 802.11ad USER ASSOCIATION TIME

Tx/Rx Distance (m)	1	4	10
Best case (ms)	146.28	153.34	172.12
Worst case (ms)	386.14	375.56	324.58
Average (ms)	247.47	245.4	243.75

### B. Beam Realignment Time

The use of directional antennas makes IEEE 802.11ad links highly susceptible to misalignment resulting from change in the orientation of devices or use movements. It is natural that if misalignment happens, device-pair tries to realign antenna beams to restore the link quality. We define the beam realignment time as the duration required by an STA and an AP to realign their beam when the alignment is disturbed. In our experiments, AP and STA were kept 1 m above the ground with a LOS connection. We rotate AP in steps of  $60^\circ$ . Fig. 4(b) illustrate an example of signal quality snapshot during the realignment duration. We can see that immediately after rotation, STA and AP try to realign their beams in order to retrieve highest achievable signal quality  $q$ . The average beam realignment time (of 20 repetition) is 7.65 ms. As opposed to existing notion that realignment can take too much time, this is a significant result showing the capability of COTS devices to quickly find the alternate beams.

### V. DEAFNESS AND INTERFERENCE

Generally, directional antennas should cause less interference to neighboring links due to the confined transmissions. However, they are highly prone to the problem of “deafness” in which transmitter of one link becomes unaware of the existing other transmission resulting in frame collisions. This is particularly a major challenge when carrier sensing based MAC protocols are used. To assess the impact of deafness, we created a measurement setup having two scenarios where two IEEE 802.11ad links (each link consists of an AP and a STA) simultaneously operate as depicted in Fig. 5(a) and (b). The distance between successive devices in both the scenarios is 1 m.

In the first scenario [see Fig. 5(a)], interfering transmitter is not able to sense the presence of primary transmitter thus creating a deaf node. In the second scenario [see Fig. 5(b)], transmitters of the primary and interfering link are facing each other, and hence both are aware of each other. Both the links use the same channel. The traffic in the primary connection was

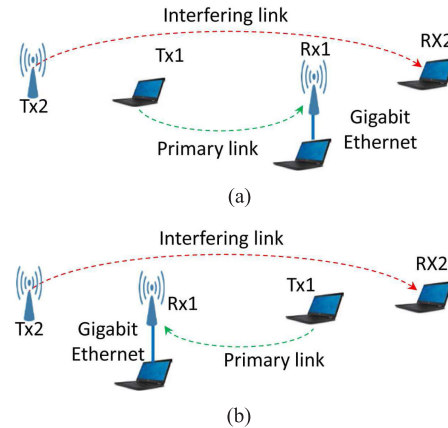


Fig. 5. Scenarios illustrating multiple IEEE 802.11ad links. (a) Interfering links with deafness. (b) Interfering links able to sense mutual transmissions.

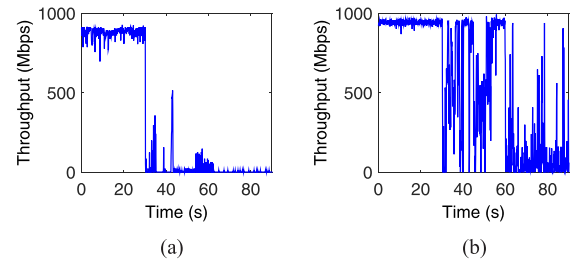


Fig. 6. Throughput performance due to co-channel interference. (a) Scenario-1. (b) Scenario-2.

generated using iPerf3. The traffic in the interfering connection was produced by the a large file transfer from the AP to STA.

Fig. 6 shows the effect of interfering link on the throughput performance of the primary link in Scenario-1 and Scenario-2, respectively. During the first 30 s, the interfering link was kept inactive active as indicated by the stable throughput of the primary link. At  $t = 30$  s, STA1 started copying large files from AP2. In Scenario-1, the collisions due to deafness result in a significant throughput degradation. The throughput remains significantly low for most of the time and cannot recover to the level before the interference was introduced. This deafness effect is a result of the directional transmission in 60 GHz. Meanwhile, in Scenario-2, the throughput degradation is not so significant which implies that both the primary and secondary transmitters are able to sense each other’s transmissions and therefore the primary link is able to coexist with the interfering link.

### VI. EFFECTS OF HUMAN BLOCKAGE

Due to small wavelength and narrow beams, 60-GHz links suffer heavily due to blockages by obstacles. The human induced shadowing is imminent in indoor environments, hence it is important to understand how the IEEE 802.11ad links behave during blockages. We designed three experimental scenarios which are likely to happen in human-induced shadowing which are as follows.

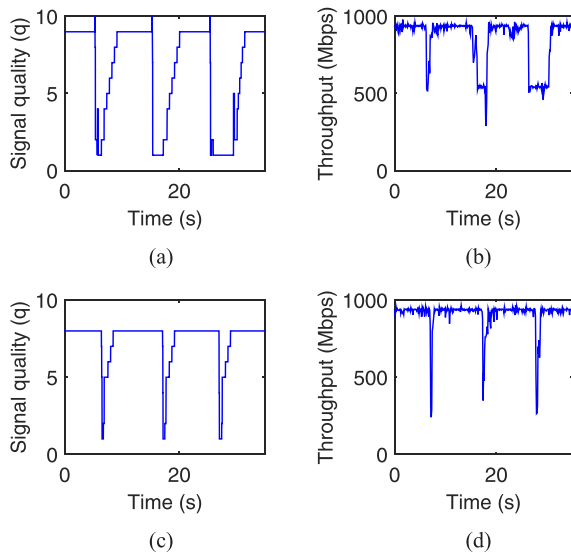


Fig. 7. Transient blockage measurements at  $d = 3$  m and  $d = 7$  m. (a) Signal quality,  $d = 3$  m. (b) Throughput,  $d = 3$  m. (c) Signal quality,  $d = 7$  m. (d) Throughput,  $d = 7$  m.

- 1) Transient human blockage, i.e., a short-term blockage caused by a person walking across an IEEE 802.11ad link.
- 2) Permanent human blockage without NLOS path, i.e., a long-term blockage caused by a human standing between an IEEE 802.11ad link, with no possibility of any reflective path.
- 3) Permanent human blockage with NLOS path availability, i.e., a long-term blockage caused by a human standing between an IEEE 802.11ad link and there is a possibility of a reflected path between the STA and AP.

Each scenario is repeated 100 times to find statistically stable measurements.

#### A. Transient Human Blockage

The transient blockage is introduced by a person walking across the 60-GHz link at normal indoor walking speed. We performed transient blockage experiment for two different distances of  $d = 3$  m and  $d = 7$  m between the STA and AP. The person walked across the link in between the AP and STA.

Fig. 7(a) and (b) shows the sample results of signal quality  $q$  (obtained from WiGig API) and throughput (obtained using iPerf) when  $d = 3$  m, respectively. Three potholes at an interval of approximately 10 s in both figures indicate the moment when a person crosses the link for three times during 35 s observation period. During the moments of obstruction, both signal quality and throughput suffer degradation as indicated by the temporary disruption of both parameters. During these moments, throughput decreases from 900 Mb/s to approximately 500 Mb/s and returns to 900 Mb/s after the obstruction is cleared from the LOS path.

Fig. 7(c) and (d) shows the sample results of signal quality  $q$  and throughput performance when  $d = 7$  m. Here, average throughput falls from above 900 Mb/s to approximately 250 Mb/s. However, the duration of disruption in the case of

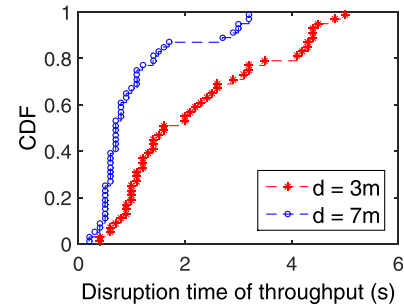


Fig. 8. CDF of throughput disruption duration for transient blockage.

$d = 7$  m is shorter than that in the case of  $d = 3$  m, although the walking speed was almost same. The reason for a sharper but lesser duration fall in the throughput when  $d = 7$  m can be explained as follows. Let us assume the beam is shaped as a cone whose apex is the transmitter. As the distance from the apex (i.e., transmitter) increases, the area of the coverage circle formed by the base of the cone increases proportionally to the square of the distance from the apex. On the other hand, the power density of transmitted signal decreases proportionally to the square of the distance. Thus when  $d = 3$  m, the coverage circle is smaller, which means the blockage duration is bound to be longer as the probability of a direct path between STA and AP is less compared to the case when  $d = 7$  m. However, since the power density of transmitted signal is higher when  $d = 3$  m, the fall in the throughput is less compared to that of  $d = 7$  m. We repeated the experiments 50 times for each of the scenarios. Fig. 8 depicts the cumulative distribution function of throughput disruption time due to the transient human blockage. The average throughput disruption time in case of  $d = 3$  m and  $d = 7$  m are 2.166 s and 1.036 s, respectively. The graph confirms that the closer the distance between STA and AP, the longer is the average shadowing duration due to the human body.

#### B. Permanent Human Blockage Without NLOS Path

The permanent blockage is represented by the presence of a human standing in between the STA and AP for a longer duration. Since there is no NLOS path the link suffers a long-term disruption.

Fig. 9(a) and (b) shows the sample result for signal quality  $q$  and throughput performance, respectively, due to the permanent blockage when  $d = 3$  m. At  $t = 7$  s, a person starts blocking the link. During the obstruction, the signal quality  $q$  falls drastically from  $q = 9$  to  $q = 2$ . On the other hand, after a sharp dip, the throughput performance is recovered and it manages to achieve the average throughput of approximately 770 Mb/s even during the blockage. A possible reason behind the throughput recovery could be the adaptive MCSs used by IEEE 802.11ad where even a lower order MCS can provide considerable data rate. Fig. 9(c) and (d) shows the signal quality  $q$  and throughput performance, respectively, for  $d = 7$  m. Here, the throughput degradation is more significant compared to the case when  $d = 3$  m. Initially throughput falls from 900 to 250 Mb/s and finally reaches 0 Mb/s at  $t = 23.4$  s, indicating that the iPerf link is disconnected. The duration when the signal quality  $q$  starts decreasing due

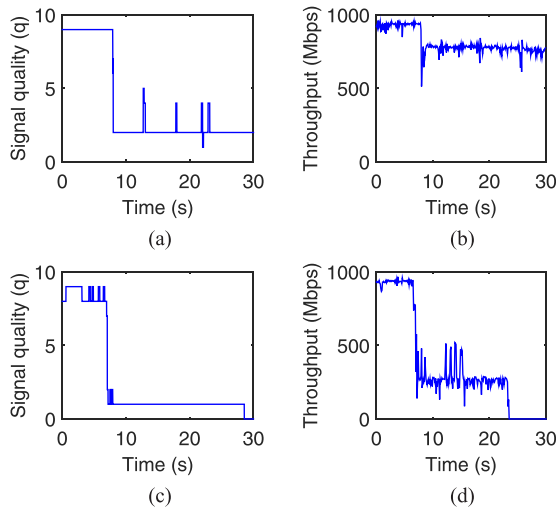


Fig. 9. Permanent blockage measurements,  $d = 3$  m,  $d = 7$  m. (a) Signal quality, 3 m. (b) Throughput, 3 m. (c) Signal quality, 7 m. (d) Throughput, 7 m.

to the presence of the obstacle until the moment when the link is disconnected is denoted as the disconnection time ( $t_{DC}$ ). From the measurement at  $d = 7$  m, the average  $t_{DC}$  is 16.329 s.

In general, the permanent blockage causes a persistent degradation in both signal quality  $q$  and throughput. As the distance between AP and the STA increases, this type of blockage can potentially break the link due to the insufficient received signal power leading to high packet loss.

### C. Permanent Human Blockage With an Alternative NLOS Path

In this scenario, STA and AP were placed 1 m away from a concrete wall. This experiment shows how the wall acting as a reflector can be exploited to provide an alternative NLOS transmission path when the LOS path is blocked. For  $d = 3$  m, Fig. 10(a) and (b) shows the sample results for signal quality  $q$  and throughput performance, respectively. When the person is in between the AP and STA, the signal quality decreases from  $q = 9$  to  $q = 4$  and fluctuates between  $q = 4$  and  $q = 6$ . The throughput performance is not significantly affected by the blockage except few small dips. The reason is that when the person obstructs the LOS transmission path, STA and AP automatically perform beam switching and take advantage of the signal reflected from the wall to establish an alternative NLOS transmission path. Since the wall is very close (1 m) to both the devices and the wall is highly reflective, high throughput performance is maintained. The signal quality  $q$  and throughput variations at  $d = 7$  m are shown in Fig. 10(c) and (d), respectively. We can observe that for  $d = 7$  m, fluctuations in the throughput are less as compared to that of  $d = 3$  m. This is because, when an obstacle is close to STA/AP, human obstructing the NLOS path eclipses the whole beam transmission area. As the distance between STA/AP and the obstacle increases, the human blocking is less likely to affect the reflected beams.

Since the highest achievable data rate is limited to 1 Gb/s due to the limitations posed by the Ethernet port of the laptop hosting

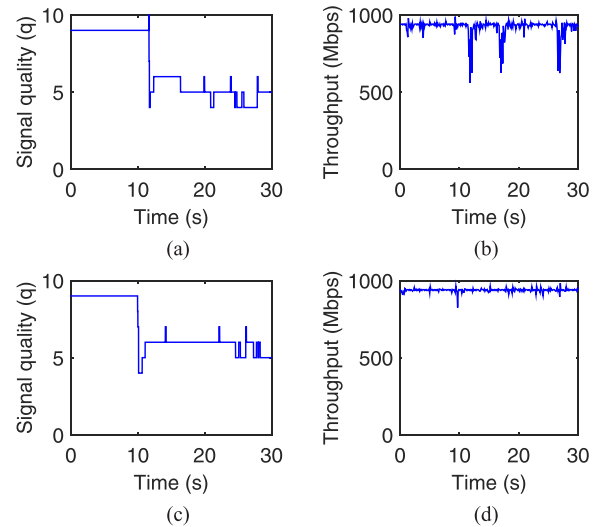


Fig. 10. Permanent blockage with NLOS path,  $d = 3$  m and  $d = 7$  m. (a) Signal quality, 3 m. (b) Throughput, 3 m. (c) Signal quality, 7 m. (d) Throughput, 7 m.

the iPerf server (for measurement purposes), the differences between the throughput performance in LOS and NLOS transmission path cannot be observed directly. If it was possible to establish 6–7 Gb/s connection, the difference among throughput of LOS and NLOS path would be higher. Nevertheless, our experiments demonstrate that even if LOS is blocked for a long duration, a 60-GHz link using COTS IEEE 802.11ad chipsets can resurrect itself by harnessing the reflective paths.

## VII. HANDOFFS IN IEEE 802.11ad WLAN

mmWave APs/BSs will be an integral part of future ultradense picocellular networks and WLANs where inter-BS/AP distances could be as low as 10 m. If the mmWave link between an STA and AP/BS is obstructed, it is highly likely that other mmWave AP/BS could be found to establish an alternate link. However, we have seen in the previous section that even if the link is blocked, the blockage can be transient in nature or an NLOS connection guaranteeing desired quality of service/experience can be established. Therefore, it is not always required to switch to an alternate AP/BS if link blockage is experienced. In the previous section, we have also seen that when  $d = 3$  m, even if a permanent human blockage occurs, the link can still function. Apart from blockages, mobility is another reason for handoffs. Thus, intelligent handoff techniques are highly desired to minimize the link disruption as well as to avoid the frequent association/disassociation with AP/BS.

### A. Blockage-Induced Handoff

In this section, we present a handoff mechanism that determines whether AP/BS switching is required or not by characterizing human blockages into the permanent blockage and transient blockage. In the case of transient blockage, STA is not required to switch to alternate AP/BS, however, if a permanent blockage occurs, the handoff is performed by switching to other



Fig. 11. Blockage induced handoff measurement setup.

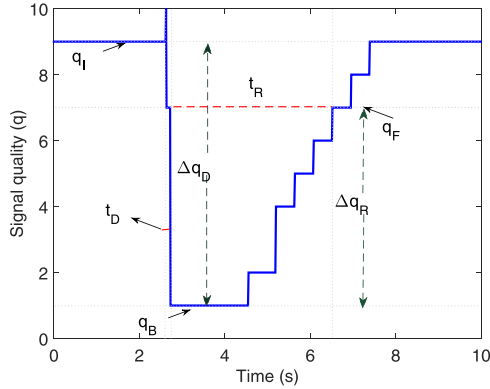


Fig. 12. Signal quality drop and recovery parameters during transient blockage.

AP/BS. We use two COTS WiGig APs and one STA as shown in Fig. 11.

1) *Parameters for Characterizing Blockage*: Let  $q_I$  be the initial signal quality when there is no shadowing. After the link is obstructed, the lowest signal quality is denoted by  $q_B$ . The difference in signal quality before and during blockage is represented by  $\Delta q_D = q_I - q_B$  units. Let  $t_D$  be the time elapsed for signal quality to drop by  $\Delta q_D$  units. If the blockage is transient or there is an NLOS path available, then signal quality will recover to some value  $q_f$  once the blockage disappear or an NLOS path is established. Let us denote the rise in the signal quality as  $\Delta q_R = q_f - q_B$  and the time required to reach  $q_f$  as  $t_R$ . Fig. 12 shows a snapshot of the transient blockage scenario with  $\Delta q_D = 8$ ,  $q_R = 6$ ,  $t_D = 160$  ms, and  $t_R = 3.789$  s.

2) *Characterizing  $t_D$  and  $t_R$* :  $\bar{t}_D$  is determined by calculating the difference between the time when blockage starts and the time at which the lowest value of signal quality  $q$  is observed. To determine recovery time  $\bar{t}_R$ , for Scenario-1 we used  $q_R = 6$  as the threshold values and for Scenario-3 we used  $q_R = 2$ . A higher  $q_R$  is chosen for Scenario-1 as we observed in the previous section that the drop in signal quality  $q$  is very significant in this case, and as the temporary blockage is over, the signal quality  $q$  increases significantly. On the other hand, in the case of Scenario-3, drop and rise in signal quality  $q$  are of small magnitudes.  $\bar{t}_R$  is not applicable to Scenario-2 as signal recovery is negligible due to the unavailability of an alternate NLOS path. However, we noticed that there are some spikes in signal quality  $q$  probably due to the ground reflections. We repeated experiments 100 times

TABLE II  
MEASURED  $t_D$  AND  $t_R$  FOR THREE BLOCKAGE SCENARIOS

		$d = 3$ m	$d = 7$ m
Transient blockage (Scenario-1)	$\bar{t}_D$	197 ms	140 ms
	$t_{D,max}$	838 ms	513 ms
	$\bar{t}_R$	3.826 s	1.648 s
Permanent blockage (Scenario-2)	$\bar{t}_D$	232 ms	298 ms
	$t_{D,max}$	748 ms	952 ms
	$\bar{t}_R$	NA	NA
	$t_{R,max}$	NA	NA
Permanent blockage with NLOS (Scenario-3)	$\bar{t}_D$	267.65 ms	411 ms
	$t_{D,max}$	707 ms	784 ms
	$\bar{t}_R$	190 ms	136 ms
	$t_{R,max}$	376 ms	313 s

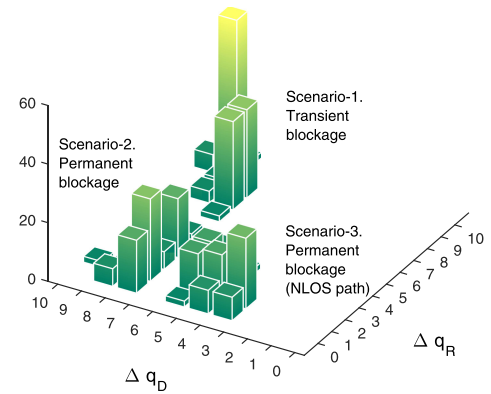


Fig. 13.  $\Delta q_D$  and  $\Delta q_R$  for each blockage scenario.

for each of the blockage scenario to characterize  $q_D$ ,  $q_R$ ,  $t_D$ , and  $t_R$ .

Table II shows the average  $t_D$  and  $t_R$ , denoted as  $\bar{t}_D$  and  $\bar{t}_R$ , respectively, for all the three scenarios. Ideally  $t_D + t_R$  is the time duration after which blockage can be categorized. However, we see that the difference in average and maximum values of  $t_D$  and  $t_R$  is quite high.

3) *Characterizing  $\Delta q_D$  and  $\Delta q_R$* : To assess  $\Delta q_D$  and  $\Delta q_R$  we set threshold on  $t_D$  and  $t_R$  as  $t_{D,th} = 1$  s and  $t_{R,th} = 3$  s based on the data from Table II such that the maximum values of  $t_D$  and  $t_R$  are included.

Fig. 13 shows the histogram of  $\Delta q_D$  and  $\Delta q_R$  for each of the blockage scenario at  $d = 7$  m. From Fig. 13, we can conclude that each blockage type has a unique  $\Delta q_D$  and  $\Delta q_R$  cluster. For example, the blockage in Scenario-1 is indicated by large  $\Delta q_D$  and  $\Delta q_R$ , while the blockage in Scenario-2 is indicated by a large  $\Delta q_D$  and a small  $\Delta q_R$ . On the other hand, blockage in Scenario-3, i.e., permanent blockage with the availability of NLOS path, both  $\Delta q_D$  and  $\Delta q_R$  have small values.

The average values of  $\Delta q_D = x_c$  and  $\Delta q_R = y_c$  for three blockage scenarios are shown in Table III. Now with this thorough characterization of the link quality for various types of blockage, we now propose a handoff algorithm.

4) *Handoff Algorithm*: The Euclidean distance ( $ED$ ) between the measured  $\Delta q_D$ ,  $\Delta q_R$  defined as  $x$  and  $y$  and the average  $x_c$

TABLE III  
 $\Delta q_D$  AND  $\Delta q_R$  MEASUREMENTS

Blockage scenario		$d = 3$ m	$d = 7$ m
Transient blockage (Scenario-1)	$\Delta q_D(x_c)$ $\Delta q_R(y_c)$	7.5 7.32	7.72 7.64
Permanent blockage (Scenario-2)	$\Delta q_D(x_c)$ $\Delta q_R(y_c)$	7.20 1.41	7.30 1.56
Permanent blockage with NLOS (Scenario-3)	$\Delta q_D(x_c)$ $\Delta q_R(y_c)$	3.40 1.13	4.06 1.20

---

**Algorithm 1: Handoff Mechanism Based on the Human Blockage Characterization.**


---

```

1: while ( $t \leq t_{D_{th}}$ ) do
2:   monitor  $\Delta q_D$ 
    $x \leftarrow \max(\Delta q_D)$ 
3: end while
4: if ( $x > 2$ ) then
5:   Blockage indication
6:   while ( $t \leq t_{R_{th}}$ ) do
7:     monitor  $\Delta q_R$ 
      $y \leftarrow \max(\Delta q_R)$ 
8:   end while
9:   calculate  $ED_1, ED_2, ED_3$ 
      $b \leftarrow \min(ED_1, ED_2, ED_3)$ 
10:  if ( $b = ED_1$  or  $b = ED_3$ ) then
11:    Short-term blockage
12:  else
13:    Long-term blockage
14:  end if
15: else
16:   No blockage
17: end if

```

---

and  $y_c$  is defined as

$$ED_i = \sqrt{(x - x_{c,i})^2 + (y - y_{c,i})^2} \quad (1)$$

where  $i \in \{1, 2, 3\}$  represent the three blockage scenarios, respectively.

The smallest  $ED_i$  implies that the measured changes in the signal quality  $q$  (i.e.,  $\Delta q_D$  and  $\Delta q_R$ ) indicate that the  $i$ th blockage scenario has occurred. The blockage characterization algorithm is described in Algorithm 1 and explained in detail as follows.

During the predefined  $t_{D_{th}}$ , a STA monitors  $\Delta q_D$  at every  $t = 1$  ms interval. If the maximum  $\Delta q_D$  exceeds 2, then there is a blockage indication. Otherwise, there is no blockage indication. We set  $\Delta q_D$  threshold to 2 but not 1 because there are always some small variations in signal quality that may result in a difference of one unit.

After detecting the blockage indication, STA monitors the  $\Delta q_R$  during the predefined  $t_{R_{th}}$ . The maximum  $\Delta q_D$  and  $\Delta q_R$  are then defined as  $x$  and  $y$ , respectively. After getting the  $x$  and  $y$  values,  $ED_1$ ,  $ED_2$ , and  $ED_3$  are calculated. The minimum distance among  $ED_1$ ,  $ED_2$ , and  $ED_3$  is indicated as the corresponding blockage type, referred to as  $b$ . If  $b$  equals to either  $ED_1$  or  $ED_3$ , then STA infers that a short-term blockage has

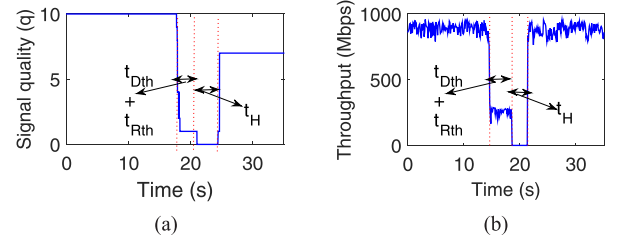


Fig. 14. Signal quality and throughput during handoff procedure. (a) Signal quality. (b) Throughput.

 TABLE IV  
 DETECTION ACCURACY FOR VARIOUS  $t_{D_{th}}$ 

$t_{D_{th}}$	$t_{R_{th}}$	$A_P$	$A_T$
250 ms	1 s	72 %	56 %
500 ms		76 %	66 %
750 ms		88 %	74 %
250 ms	3 s	96 %	73 %
<b>500 ms</b>		<b>97 %</b>	<b>96 %</b>
750 ms		99 %	97 %
250 ms	6 s	100 %	72 %
500 ms		96 %	92 %
750 ms		100 %	96 %

happened. Otherwise, a long-term blockage is indicated which is followed by handoff initiation.

Fig. 14(a) and (b) demonstrates the signal quality and throughput variation during the handoff triggered due to a permanent blockage. The total time taken in a blockage-induced handoff procedure consist of  $t_{D_{th}} + t_{R_{th}} + t_H$ . From our handoff experiments, we found that average  $t_H$  is 2.749 s. Since we used  $t_{D_{th}} = 1$  s and  $t_{R_{th}} = 2$  s, the average time to switch the AP is 6.749 s.

5) *Accuracy of Blockage Detection:* We observe that the proposed blockage characterization relying on the fluctuations in signal quality parameters ( $\Delta q_D$ ,  $\Delta q_R$ ) mainly depends on the threshold observation durations  $t_{D_{th}}$  and  $t_{R_{th}}$ . Hence, its important to determine the accuracy of characterization. We define  $A_T$  and  $A_P$  as the accuracy of detecting transient blockage and permanent blockage, respectively. To assess the impact of  $t_{D_{th}}$  and  $t_{R_{th}}$  on  $A_T$  and  $A_P$ , performed experiments considering multiple  $t_{D_{th}}$  and  $t_{R_{th}}$ . We performed 50 measurements for each combination of  $t_{D_{th}}$  and  $t_{R_{th}}$  for each of the blockage type. Table IV shows the accuracy of blockage type detection for different values of  $t_{D_{th}}$  and  $t_{R_{th}}$ . We can observe that when  $t_{R_{th}} = 1$  s false detection is particularly high for the transient blockage scenario. This is because the transient blockage is characterized by a high  $\Delta q_D$  as well as a high  $\Delta q_R$ . However, a smaller recovery time threshold may not allow enough rise in signal quality  $q$ . This results in interpreting transient blockage as the permanent one. The accuracy in detection of permanent blockage is generally high. As  $t_{R_{th}}$  and  $t_{D_{th}}$  increase, the accuracy of both blockage types detection increase. A large  $t_{R_{th}} + t_{D_{th}}$  means delay in handoff decision, which can result in a low QoS/QoE if link is obstructed by the permanent blockage. It appears that  $t_{R_{th}} = 500$  ms and  $t_{D_{th}} = 3$  s provide reasonably high accuracy.



Fig. 15. Experimental scenario for handoff triggered by corner effects.

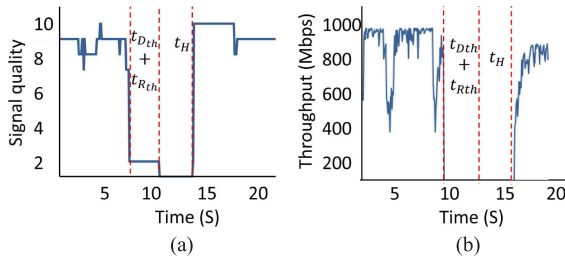


Fig. 16. Handoff between AP located in the room and in the corridor. (a) Signal quality. (b) Throughput.

### B. Mobility-Induced Handoff in Indoors

One of the important characteristics of 60-GHz-based picocells in an indoor environment is the limited overlap area between neighboring APs which is also called corner effect. This is one of the main hurdle in providing a WiFi-like seamless indoor coverage at 60-GHz frequency band.

Fig. 15 shows such a scenario we used for our experiments. AP1 is placed at the ceiling of office room while AP2 is in the ceiling of corridor. Initially, STA is in the room and connected with AP1. Fig. 16 shows the signal quality  $q$  and corresponding iPerf throughput variation when the STA connected with AP1 walks out of the room. As soon as STA crosses the door and reaches behind the wall, a sudden dip in the signal quality  $q$  and throughput is observed, although the traveled distance is only 2–2.5 m. This phenomenon is not observed in 2.4/5 GHz as signals can easily penetrate walls. For our handover mechanism, as soon the signal quality falls below  $q = 2$ , STA disassociates itself (assuming a permanent blockage) with AP1 and is able to connect with the AP2 located in the corridor in 3 s.

### C. Comments on the Measured Handoff Delay

Generally, when an STA moves away from the connected AP, the signal quality decreases. In traditional IEEE 802.11 WLANs, if signal quality decreases below a certain threshold, the STA sends the probe packets to confirm the presence of other APs. The exchange of probe request and response messages constitutes the discovery phase. Once the STA has discovered an alternate AP, authentication and association procedures are followed. Let the delays incurred in discovery, authentication, and association be represented by  $t_{dis}$ ,  $t_{auth}$ , and  $t_{as}$ , respectively. In the proposed IEEE 802.11ad handoff mechanism, the additional

delay in making handoff decision (due to the characterization of blockage type), i.e.,  $t_{R_{th}} + t_{D_{th}}$  is also involved. Thus, the total delay  $t_s$  incurred in switching from one AP to another AP can be defined as

$$t_s = t_{R_{th}} + t_{D_{th}} + t_{dis} + t_{auth} + t_{as}. \quad (2)$$

Here,  $t_H = t_{dis} + t_{auth} + t_{as}$  as shown in Fig. 16. The measured average switching time in our experiments is 6.749 s, which is quite high compared to the legacy IEEE 802.11 WLANs where it generally takes less than a second in handoffs. The main reasons behind fast handoffs in WiFi are as follows.

- 1) WiFi STAs always keep a list of alternate APs which reduces the discovery delay.
- 2) Inter-AP connectivity in WiFi networks greatly reduces the association and authentication delay.
- 3) Blockage characterization and beam-searching are not needed.

An important reason behind the high handoff delay could be that the docking stations we used in our experiments are not optimized for WLANs operations. To provide seamless multi-Gb/s wireless connectivity, smooth handoffs are a must for next generation of 60-GHz systems. This requires better network design approaches particularly considering the above listed factors and a possibly close-integration with the sub-6-GHz air-interfaces.

## VIII. CONCLUSION

Among millimeter wave (mmWave) frequencies, 60-GHz band is leading in terms of research efforts and the availability of commercial devices. The inevitability of mmWave communications in future networks warrants careful performance evaluation of commercial off-the-shelf (COTS) 60-GHz devices. This article presented an experimentation driven extensive measurements based work. We carefully designed scenarios and through thorough practical evaluation, we provided important insights about the directional antenna patterns, alignment, and association overheads and interference and blockage characteristics of COTS IEEE 802.11ad devices from a WLAN/picocell perspective where frequent handoffs can be triggered. Through multiple measurements, we have provided a highly accurate (96%–97%) blockage characterization mechanism to assist link blockage-induced handoffs. Our in-depth analysis of human blockage shows that it is important to differentiate between the blockage types to avoid unnecessary handoffs. Our insights, backed by accurate quantitative measurement data, are highly beneficial in designing and improving the efficiency of next generation mmWave networks. The detailed experimentation results provided in this article can act as a benchmark for future design of indoor 60-GHz picocells.

## REFERENCES

- [1] T. Rappaport *et al.*, “Millimeter Wave mobile communications for 5G cellular: It will work!” *IEEE Access*, vol. 1, pp. 335–349, 2013.
- [2] K. Chandra, R. V. Prasad, B. Quang, and I. G. M. M. Niemegeers, “Cogcell: Cognitive interplay between 60 GHz picocells and 2.4/5 GHz hotspots in the 5G era,” *IEEE Commun. Mag.*, vol. 53, no. 7, pp. 118–125, Jul. 2015.

- [3] K. Chandra, A. Doff, Z. Cao, R. V. Prasad, and I. Niemegeers, “60 GHz MAC standardization: Progress and way forward,” in *Proc. 12th Annu. IEEE Consum. Commun. Netw. Conf.*, Jan. 2015, pp. 182–187.
- [4] M. Jacob, S. Priebe, A. Maltsev, A. Lomayev, V. Erceg, and T. Kurner, “A ray tracing based stochastic human blockage model for the IEEE 802.11ad 60 GHz channel model,” in *Proc. 5th Eur. Conf. Antennas Propag.*, 2011, pp. 3084–3088.
- [5] K. Chandra, R. V. Prasad, and I. Niemegeers, “Performance analysis of IEEE 802.11ad MAC protocol,” *IEEE Commun. Lett.*, vol. 21, no. 7, pp. 1513–1516, Jul. 2017.
- [6] Y. Zhu *et al.*, “Demystifying 60 GHz outdoor picocells,” in *Proc. 20th Annu. Int. Conf. Mobile Comput. Netw.*, Maui, HI, USA, 7–11 Sep. 2014, pp. 5–16.
- [7] S. K. Saha, V. V. Vira, A. Garg, and D. Koutsonikolas, “60 GHz multi-gigabit indoor WLANs: Dream or reality?” 2015, *arXiv:1509.04274*.
- [8] T. Nitsche, G. Bielsa, I. Tejado, A. Loch, and J. Widmer, “Boon and bane of 60 GHz networks: Practical insights into beamforming, interference, and frame level operation,” in *Proc. 11th ACM Conf. Emerg. Netw. Exp. Technol.*, 2015, pp. 17:1–17:13.
- [9] S. Sur, V. Venkateswaran, X. Zhang, and P. Ramanathan, “60 GHz indoor networking through flexible beams: A link-level profiling,” in *Proc. ACM SIGMETRICS Int. Conf. Meas. Model. Comput. Syst.*, 2015, pp. 71–84.
- [10] S. Sur, X. Zhang, P. Ramanathan, and R. Chandra, “BeamSpy: Enabling robust 60 GHz links under blockage,” in *Proc. 13th USENIX Symp. Netw. Syst. Des. Implementation*, 2016, pp. 193–206.
- [11] J. Zhang, X. Zhang, P. Kulkarni, and P. Ramanathan, “Openmili: A 60 GHz software radio platform with a reconfigurable phased-array antenna,” in *Proc. ACM Mobicom*, 2016, pp. 162–175.
- [12] H. Hassanieh, O. Abari, M. Rodreguez, M. Abdelghany, D. Katabi, and P. Indyk, “Agile millimeter wave networks with provable guarantees,” 2017, *arXiv:1706.06935*.
- [13] S. K. Saha, L. Sun, and D. Koutsonikolas, “Improving connectivity, coverage, and capacity in 60 GHz indoor WLANs using relays,” in *Proc. Workshop Wireless Students Students Students*, 2015, pp. 35–37.
- [14] J. Ansari, N. Perpinias, A. Nahring, P. Mahonen, and M. Petrova, “Empirical characterization of mm-wave communication links in realistic indoor scenarios,” in *Proc. IEEE Wireless Commun. Netw. Conf.*, 2015, pp. 1799–1804.
- [15] A. Loch, “Millimeter-wave blind spots: Mitigating deafness collisions using frame aggregation,” in *Proc. IEEE Conf. Comput. Commun. Workshops*, 2016, pp. 158–163.
- [16] J. Palacios, D. De Donno, and J. Widmer, “Tracking mm-wave channel dynamics: Fast beam training strategies under mobility,” in *Proc. IEEE INFOCOM*, 2017, pp. 1–9.
- [17] L. Simić, N. Perpinias, and M. Petrova, “60 GHz outdoor urban measurement study of the feasibility of multi-Gbps mm-Wave cellular networks,” in *Proc. IEEE Conf. Comput. Commun. Workshop*, Mar. 2016, pp. 331–336.
- [18] M. K. Haider and E. W. Knightly, “Mobility resilience and overhead constrained adaptation in directional 60 GHz WLANs: Protocol design and system implementation,” in *Proc. 17th ACM Int. Symp. Mobile Ad Hoc Netw. Comput.*, 2016, pp. 61–70.
- [19] I. Corporation, “Intel Wireless Gigabit Sink W13100 Product Brief.” [Online]. Available: <http://www.intel.com/content/www/us/en/wireless-products/wigig-sink-w13100-brief.html>
- [20] I. Corporation, “Intel Tri-Band Wireless-AC 17265 Product Brief.” [Online]. Available: <http://www.intel.com/content/www/us/en/wireless-products/tri-band-wireless-ac17265-brief.html>
- [21] “iPerf - The TCP, UDP, and SCTP network bandwidth measurement tool,” [Online]. Available: <https://iperf.fr/>
- [22] S. K. Saha *et al.*, “Fast and infuriating: Performance and pitfalls of 60 GHz WLANs based on consumer-grade hardware,” in *Proc. 15th Annu. IEEE Int. Conf. Sens., Commun., Netw.*, Hong Kong, 2018, pp. 1–9.